Available online at www.sciencedirect.com
SCIENCE DIRECT®
Electrochimica Acta 49 (2004) 4589–4597
ELECTROCHIMICA Acta
www.elsevier.com/locate/electacta

# Nanostructured CuO thin film electrodes prepared by spray pyrolysis: a simple method for enhancing the electrochemical performance of CuO in lithium cells

Julián Morales[a], Luis Sánchez[a,*], Francisco Martín[b], Jose R. Ramos-Barrado[b], Miguel Sánchez[b]

[a]*Departamento de Química Inorgánica e Ingeniería Química, Facultad de Ciencias, Campus de Rabanales, Edificio Marie Curie, Universidad de Córdoba, 14071 Córdoba, Spain*
[b]*Laboratorio de Materiales y Superficie (Unidad Asociada al CSIC), Universidad de Málaga, Spain*

Received 22 December 2003; received in revised form 7 May 2004; accepted 8 May 2004

Available online 19 June 2004

**Abstract**

Nanostructured CuO thin films were prepared by using a spray pyrolysis method, copper acetate as precursor and stainless steel as substrate. The textural and structural properties of the films were characterized by scanning electron microscopy (SEM), atomic force microscopy (AFM), X-ray diffraction (XRD) and X-ray photoelectron spectroscopy (XPS). The SEM images revealed thorough coating of the substrate and thickness of 450–1250 nm; the average particle size as determined from the AFM images ranged from 30 to 160 nm. The XRD patterns revealed the formation of CuO alone and the XPS spectra confirmed the presence of $Cu^{2+}$ as the main oxidation state on the surface. The films were tested as electrodes in lithium cells and their electrochemical properties evaluated from galvanostatic and step potential electrochemical spectroscopy (SPES) measurements. The discharge STEP curves exhibited various peaks consistent with the processes CuO $\Leftrightarrow$ $Cu_2O$ $\Leftrightarrow$ Cu and with decomposition of the electrolyte, a reversible process in the light of the AFM images. The best electrode exhibited capacity values of 625 Ah $kg^{-1}$ over more than 100 cycles. This value, which involves a CuO $\Leftrightarrow$ Cu reversible global reaction, is ca. 50% higher than that reported for bulk CuO. The nanosize of the particles and the good adherence of the active material to the substrate are thought to be the key factors accounting for the enhanced electrochemical activity found.


*Keywords:* Copper oxide; Thin films; Rechargeable lithium batteries; Negative electrode

## 1. Introduction

In recent years, extraordinary efforts have been made at finding alternative anodic materials to replace carbon-based materials in Li-ion batteries. One special contribution in this context was the development of the Stalion® lithium-ion cell [1] by Fuji Photo Film Celltec. Co. (Japan). Notwithstanding its limited commercial success, the results [2] were widely celebrated by the scientific community as they opened up new avenues in the search of alternative materials. These studies revealed a high specific capacity in tin-based systems used as anode materials due to their ability to form $Li_xSn$ reversible alloys ($1.0 < x < 4.4$). These findings have revived interest in traditional and new materials reacting reversibly with lithium at low potentials, and drew special attention to those based on tin [3,4], silicon [5] and intermetallic alloys [6–8]. Two major drawbacks remains to be overcome with a view to facilitating their use in the manufacture of lithium batteries, namely: (i) a significant irreversible capacity loss during the first discharge–charge cycle (particularly in oxide-based systems); and (ii) the poor capacity retention resulting from Li-alloying agglomeration.

* Corresponding author. Tel.: +34 957 218620; fax: +34 957 218621.
*E-mail address:* luis-sanchez@uco.es (L. Sánchez).

0013-4686/$ – see front matter © 2004 Elsevier Ltd. All rights reserved.
doi:10.1016/j.electacta.2004.05.012

An alternative approach to the development of anodic materials have been recently reported by Poizot et al. [9]. They found 3d-transition metal oxides ($M_xO_y$, M = Co, Ni, Cu, Fe) to reversibly react with Li ions at low potentials. A simple, yet brilliant, lithium reaction mechanism was put forward to account for the reversibility observed [9–11] and summarized by the simple reaction:

$$M_xO_y + 2yLi \Leftrightarrow xM + yLi_2O. \quad (1)$$

The $Li_2O$ formed in the reduction process behaves as an electrochemically active material in the reverse reaction. The origin of this behaviour, previously unknown, was ascribed to the nanometric nature of the metal particles formed. It is thus believed that, in this aggregation state, the particles possess and enhanced electrochemical reactivity towards the formation/decomposition of $Li_2O$ [9]. In fact, nanostructured materials have emerged as attractive alternatives to conventional materials by virtue of their prominent electronic and chemical properties [12]. These transition metal oxides can retain capacity values as high as 700 Ah $kg^{-1}$ on extended cycling. These values clearly exceed those of graphite-based anodic materials (theoretical gravimetric capacity 372 Ah $kg^{-1}$) and have been deemed future candidates to replacing these carbonaceous materials. Thus, various transition metal oxides ($Co_3O_4$ [11,13–15], $Fe_2O_3$ [16], $LiFeO_2$ [17], $Li_5FeO_4$ [17]) were recently examined as anodic materials for Li-ion batteries. This idea was first suggested for $Fe_2O_3$ by Morzilli et al. [18], who did not address the reaction mechanism involved, however.

Among these transition metal oxides, CuO possesses attractive advantages. Thus, it is an inexpensive, non-toxic compound used in the manufacture of Li/CuO primary cells [19,20]. Recently, the electrochemical reactivity of CuO towards lithium was revisited by Débart et al. [21] demonstrated the reversibility of reaction (1) for CuO, which involves the formation of $Li_2O$, Cu and $Cu_2O$ nanograins as intermediates. However, Grugeon et al. [10] found that the CuO cell to deliver a sustained reversible capacity of only ca. 400 Ah $kg^{-1}$ (i.e. similar to that observed for $Cu_2O$) upon extended cycling. This means that more than a 50% of the CuO theoretical capacity, referred to its reduction to Cu, is unavailable.

The spray pyrolysis method is a well-known nanostructured thin-film preparation method with excellent features such as the need for no sophisticated equipment, and quality targets or substrates; also, film thickness and stoichiometry are easy to control and the resulting films are well compacted. We have used this coating method to prepare thin films of nanosize active material for lead–acid and lithium batteries [22,23]. In this work, we extended this method to the preparation of nanocrystalline CuO thin films and explored their activity as electrodes in lithium batteries. This synthetic procedure results improves the electrochemical reactivity of CuO compared with the bulk material. The reversibility of the CuO ⇔ Cu reaction is enhanced and the cell can deliver high, sustained specific capacity values upon extended cycling.

## 2. Experimental

A previously reported spray pyrolysis method [24], was used to prepare the CuO coatings. An aqueous solution of 0.05 M $Cu(CH_3COO)_2$ was used as precursor. The solution was pumped into the air stream in the spray nozzle at a rate of 50 mL $h^{-1}$ by means of a syringe pump, for a preset time of 30 and 80 min. An air stream of 25 L $min^{-1}$, measured at 1.25 bar, was used to atomize the solution. Circular disks of commercial 304 stainless steel (0.4 mm thick and 7.5 mm in diameter) were used as substrate. They were kept at temperatures over the range of 200–300 °C. The amount of oxide attached to the substrate was determined by weighting the electrode before and after deposition using a Sartorius microbalance with a sensitivity of ±1 μg. X-ray diffraction (XRD) patterns were recorded on a Siemens D5000 X-ray diffractometer, using Cu Kα radiation and graphite monochromator, in steps of 0.02° and 1.2 s. Scanning electron microscopy (SEM) images were obtained on a Jeol JMS-5300 microscope. Topographic AFM examinations were performed by using a Nanoscope IIIa contact-mode AFM (Digital Instruments). Type NP cantilevers (Digital Instruments) with $Si_3N_4$ tips and a spring constant of 0.58 N $m^{-1}$ were employed. In order to avoid exposure to the air, a series of precautions were adopted in recording the AFM images of the discharged and charged electrodes. Thus, the electrodes were covered with a layer of propylene carbonate inside of a dry-box and rapidly transferred to the liquid cell of the AFM microscope. In this manner, the electrode surface is protected against the exposure to water or oxygen during the measurement and the results must reflect the changes undergone by the electrode surface inside the electrochemical cell.

X-ray photoelectron and X-ray excited Auger spectra were obtained with a Physical Electronics PHI 5700 spectrometer using non-monochromated Mg Kα radiation ($h\nu$ = 1253.6 eV) and a hemispherical analyser operating at constant pass energy of 29.35 eV. Spectra were recorded with the X-ray generator operated at 15 kV and 20 mA. The energy scale of the spectrometer was calibrated using the Cu $2p_{3/2}$, Ag $3d_{5/2}$ and Au $4f_{7/2}$ photoelectron lines at 932.7, 368.3 and 84.0 eV, respectively. The vacuum in the analysis chamber was better than $10^{-9}$ mbar. Binding energies were corrected using the binding energy values for C 1s of adventitious carbon (and for the methyl group) fixed at 284.8 eV. Samples were mounted on a holder without adhesive tape and kept under high vacuum in the preparation chamber overnight before they were transferred to the analysis chamber of the spectrometer. Survey spectra over the range 0–1200 eV were recorded at a 187.85 pass energy, each region being scanned several times to ensure an

adequate signal-to-noise ratio. A 3 mm × 3 mm sample area was sputtered with 4 keV $Ar^+$; the sputter rate was assumed to be ∼0.3 nm $min^{-1}$ as determined for $Ta_2O_5$ under identical sputtering conditions. Spectra were processed using PHI-Access V.6 and Multipak software, both from Physical Electronics. Curve fitting of high-resolution spectra was done after Shirley background correction and satellite subtraction. Surface atomic concentrations were determined from peak areas, using Shirley background subtraction and sensitivity factors provided by the spectrometer manufacturer (Physical Electronics, Eden Prairie, MN). In order to avoid the reduction of copper oxide by the X-ray as far as possible, the data for the Cu 2p region were collected at short acquisition times. For ex situ XPS measurements once the cell was dismantled, the pellet was washed with hexane. All these manipulations were performed in argon atmosphere and a special glove-box connected to the antechamber of the spectrometer allowed to transfer the sample into the spectrometer avoiding a direct contact with air.

Electrochemical measurements were carried out in two electrodes cells, using lithium as counter-electrode. The electrolyte used was Merck battery electrolyte LP 40 (EC:DEC = 1:1 (w/w) 1 M $LiPF_6$). Circular disks of stainless steel coated with the active material were used as working electrodes. The cells were galvanostatically charged and discharged at a current density of 0.075 mA $mg^{-1}$ (*C*/5 cycling rate, *C* being defined as one $Li^+$ exchanged in 1 h). The SPES curves were recorded with regime of 75 mV $h^{-1}$ per step. All electrochemical measurements were controlled via a MacPile II potentiostat–galvanostat.

## 3. Results and discussion

Different coatings were prepared by changing the heating temperature of substrate and the time of deposition of the copper(II) acetate solution. Fig. 1 shows the XRD patterns for the samples prepared under the experimental conditions shown in Table 1. The low signal to noise ratio reveals a low crystallinity in the samples. The XRD patterns exhibit two main signals at 35.6° and 38.7° 2$\theta$ that can be ascribed to the (−1 1 1) and (1 1 1) reflections of the CuO phase [25]. Peak intensities and hence crystallinity increased with increasing temperature and, especially, increasing deposition time. Although the low crystallinity of the particles, reflected in

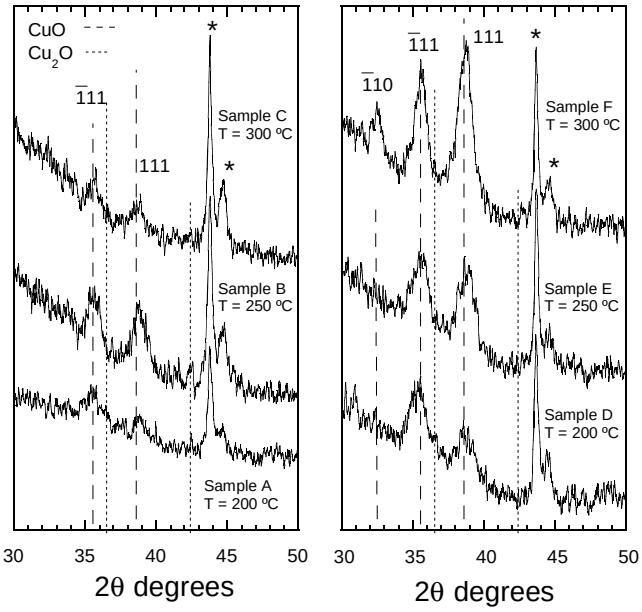


Fig. 1. XRD patterns for CuO thin films. The asterisk denotes diffraction lines corresponding to the substrate.

substantial broadening of peaks, precluded the accurate identification of the $Cu_2O$ phase in the films, the absence of the (1 1 1) reflection, located at a rather different spacing from those of CuO, allows one to discard its formation under the deposition conditions used.

SEM images revealed thorough coating of the substrate. The films are highly dense and uniform, which makes it difficult to distinguish individual particles. The values of the film thickness, estimated from cross-sectional SEM images (Fig. 2a), are shown in Table 1. Complementary information of the film morphology was obtained from AFM images, which also exposed the high uniformity of the films obtained with all the treatments and revealed that they resulted from the agglomeration of round-shape nanoparticles (see Fig. 2b). Particle size was calculated by averaging the results of several AFM observations in different regions of the films (Table 1). The evaluation of the crystallite size from the main reflections of the XRD patterns was hindered by the low resolution of the peaks. Only for sample F, where crystallinity is clearly enhanced, one can obtain reasonably accurate values. Crystallite size obtained from

Table 1
Experimental preparation conditions and physical characteristics of the CuO thin films

| Sample | Temperature (°C) | Time (min) | Mass deposited (mg $cm^{-2}$) | Thickness[a] (nm) | Particle size[b] (nm) |
|---|---|---|---|---|---|
| A | 200 | 30 | 0.36 | 660 | 20–60 |
| B | 250 | 30 | 0.30 | 475 | 40–75 |
| C | 300 | 30 | 0.17 | 420 | 25–60 |
| D | 200 | 60 | 0.58 | 1100 | 80–200 |
| E | 250 | 60 | 0.56 | 1150 | 60–180 |
| F | 300 | 80 | 0.73 | 1250 | 100–220 |

[a] Estimated from SEM images.
[b] Estimated from AFM images.

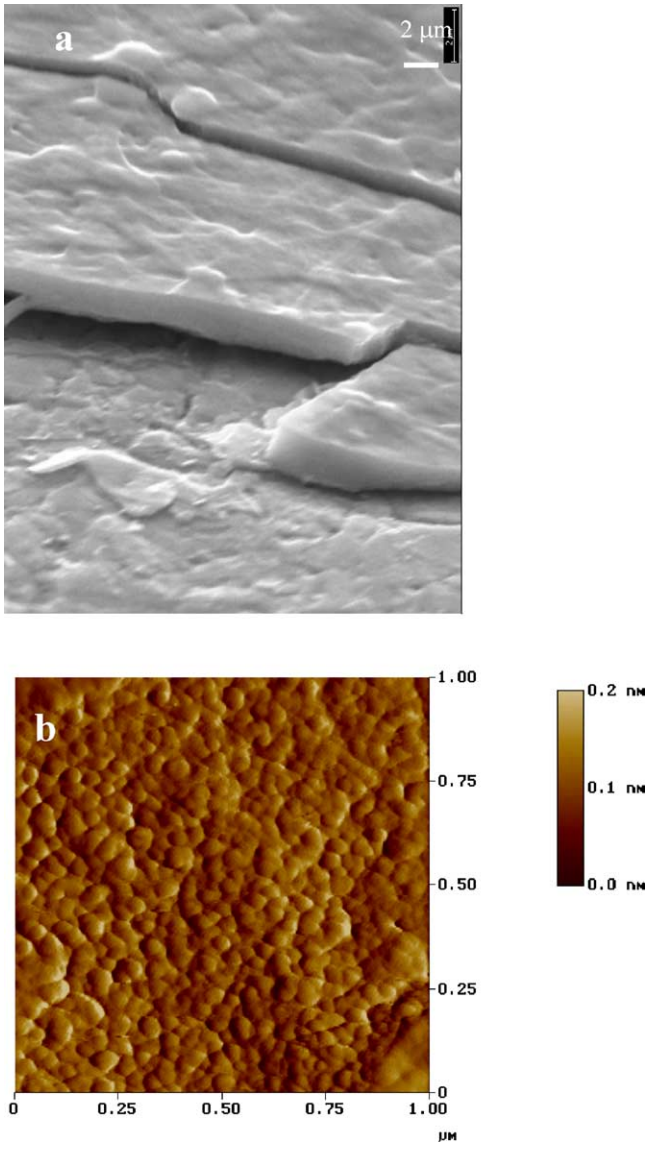


Fig. 2. SEM (a) and AFM (b) images of CuO thin film (sample B).

(1 1 1) reflection was ca. 10 nm, notably smaller than particle size obtained from microscopy images. This means that the nanograins are built up of several coherent diffraction domains. The influence of the experimental synthetic conditions on film growth was as follows: (i) On identical deposition times, the amount deposited decreased with increasing the temperature. This phenomenon has often been observed in the preparation of various materials by spray pyrolysis, probably because the drop of the precursor solution burst and spilled part of its component off the substrate [26]. (ii) Particle size and film thickness increased with increasing deposition time. (iii) The increase of temperature only affects to the crystallinity of the samples, especially to those obtained after large periods of deposition.

Fig. 3 shows the Cu 2p, O 1s and C 1s XPS spectra. No other signals belonging to Fe, Cr or Ni, the main elements constituent the substrate, were detected, which provides additional evidence of the complete, uniform coating of the substrate. The well-defined shake-up satellite structures observed at ca. 7 and 9.5 eV on the high binding energy side of the copper core line $2p_{3/2}$ (centred at 934 eV) is typical of $Cu^{2+}$ species and due to multiplet splitting. Moreover, the Cu $L_3M_{4.5}M_{4.5}$ Auger signal centred at a kinetic energy of 917.8 eV [27] (not included in Fig. 3) is also consistent with the presence of $Cu^{2+}$ as the dominant species on the surface. However, the Cu $2p_{1/2}$ and $2p_{3/2}$ peaks are relatively broad and seem to be influenced by the presence of $Cu_2O$ and/or other copper species (e.g. residual copper acetate). Also, the C and O 1s peaks exhibit different components, which indicates that these atoms lie in different chemical environments.

In order to obtain a more accurate knowledge about these environments, peaks were fitted using a Gaussian–Lorentzian mixed function. The most representative species found were as follows: (i) CuO (933.7 eV Cu $2p_{3/2}$ and 529.6 eV O 1s) [28]; (ii) $Cu_2O$ (932.5 eV Cu $2p_{3/2}$ and 530.3 eV O 1s) [28]. The peak intensity of this latter phase was very weak and changed little with the deposition time or temperature, so the $Cu_2O$ content can scarcely be affected by these parameters as $Cu_2O$ results from the reduction of $Cu^{2+}$ by X-rays [29]; (iii) copper acetate (935.6 eV Cu $2p_{3/2}$, 288.3 eV C 1s and 531.9 and 533 eV O 1s); (iv) adventitious carbon (284.8 eV C 1s); and (v) hydroxyl groups (531.2 eV O 1s). The surface composition of these films is shown in Table 2. Although the carbon content calculated from the C 1s signal is significant, ca. 20–40%, most is adventitious carbon coming from contamination of different origin: vacuum pumps, handling, etc. The fraction belonging to undecomposed acetate can be calculated from the peak at 288.3 eV, assigned to the carboxylate group $–COO^-$. The area of this peak is ca. 30% of the total C 1s signal. Thus, for sample A, about 7% of the total carbon should be as acetate and directly bound to copper. The remainder should be adventitious carbon. So, a 3.5% of copper should be as undecomposed copper acetate. As expected, the intensity of all peaks related to the presence of undecomposed copper acetate and water-containing species decreased with increasing deposition temperature. Moreover, the layer of undecomposed material is indeed very thin, as shown by the spectra obtained after 20 s of $Ar^+$-ion sputtering and consistent with the surface atomic concentration results. The most salient changes were a significant drop in C content

Table 2
Results of the XPS elemental analysis (%) of the thin films synthetized

| Sample | C | O | Cu |
|---|---|---|---|
| A | 23 (3.5) | 43 (29.5) | 34 (67) |
| B | 25 (3.0) | 42 (29.0) | 33 (68) |
| C | 19 (4.5) | 43 (30.5) | 38 (65) |
| D | 28 (3.5) | 42 (29.5) | 30 (67) |
| E | 42 (3.0) | 38 (29.0) | 20 (68) |
| F | 33 (4.5) | 39 (30.5) | 28 (65) |

The values in parentheses were obtained upon ion-etching for 20 s.

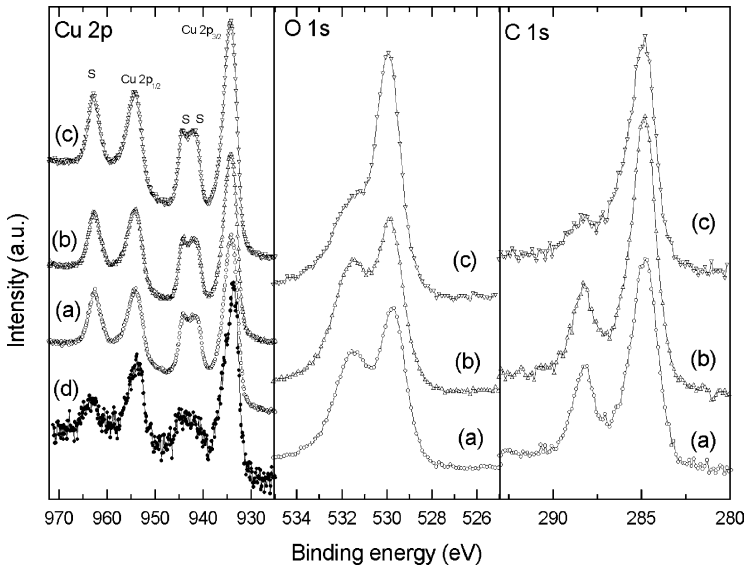


Fig. 3. XPS Cu 2p, O 1s and C 1s core level spectra for the following samples: (a) A; (b) B; (c) C; (d) A after the first charge up to 3.0 V.

(3–4%, see Table 2), with virtually complete disappearance of the C 1s peak at 288.3 eV, and a rise in Cu content to almost twice that of O. This means that the surface composition approaches that of $Cu_2O$ as a consequence of the instability of the $Cu^{2+}$ species to $Ar^+$-ion bombardment and their transformation into cuprite. By assuming a depth value of 10 nm $min^{-1}$ of ion $Ar^+$ etching [30], the layer thickness of the undecomposed acetate should be around 3 nm. Taking into account the total thickness of the coatings, the copper content as copper acetate should be below 0.01%. This is an outstanding result concerning to the electrochemical behaviour of these films in lithium cells, because their response in these devices will be essentially ascribed to CuO, the major component.

The electrochemical tests were performed on samples A, B and F prepared at three different temperatures. Samples A and F have the smallest and the biggest particle sizes, respectively, whereas sample B has a somewhat smaller thickness and bigger particle size than sample A. Fig. 4 shows the first galvanostatic discharge–charge and the second discharge curve for various Li/CuO cells. The first discharge curve for samples A and F exhibits an abrupt drop in the potential up to 1.4−1.2 V, with a small sloping change below 2.5 V that is better defined for sample F and followed by two pseudo-plateaux centred at 1.3−1.1 and 0.9−0.8 V. These plateaux were even better defined for the second discharge curve, being this latter behaviour common of all samples. The voltage curve profiles resemble those reported for bulk CuO [10,21] except that, in our samples, the plateaux of the second discharge are better defined. The samples A and B exhibited capacity values greater than that predicted for the theoretical CuO → Cu reduction process, and only sample F, which contains a greater amount of active material, approaches the theoretical value of two lithium ions per mole of compound. The presence of impurities of other transition metals accounting for the abnormal first discharge capacity observed can be discarded in the light of the XPS results. Our results resemble those of Laik et al. [31]

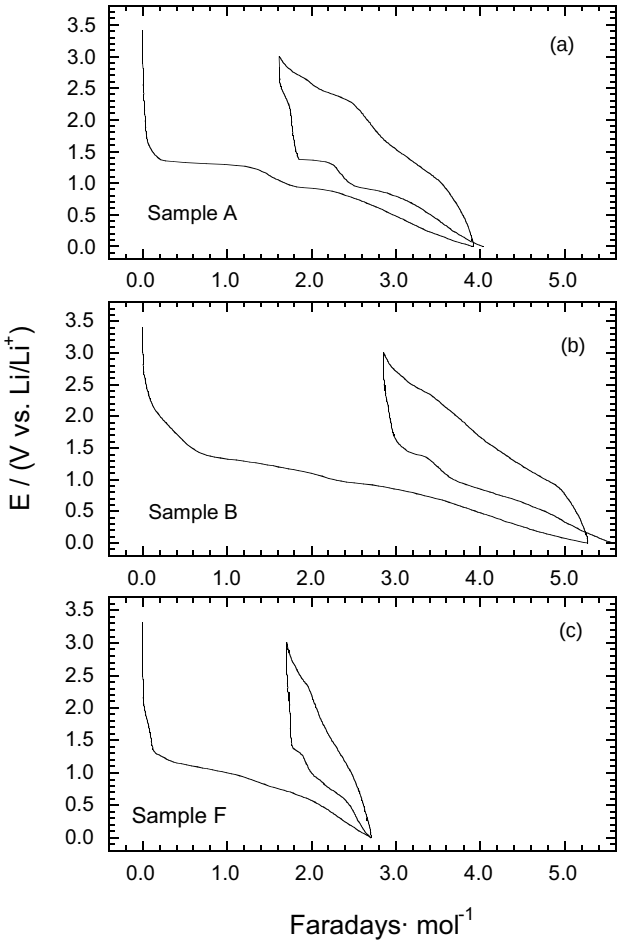


Fig. 4. First galvanostatic curves for Li/CuO cells.

for a $Cu_2O$ anode material grown on Ti-plated quartz crystals. The number of inserted lithium atoms in the first discharge to a cut-off potential of 0 V was slightly greater than 5, which substantially exceeds the theoretical value of 2. The additional discharge was ascribed to electrolyte reduction. All charge curves exhibited a strong polarization, with subtle sloping changes. The cells tended to remove about two $Li^+$ per unit formula at a cut-off voltage of 3.0 V; by exception, the charge capacity for sample F corresponded to the removal of 1.0 $Li^+$ per unit formula.

The participation of the electrolyte in the global electrochemical process of these thin film electrodes seems to play a major role. For these types of electrodes, the formation of a solid electrolyte interphase (SEI) has been suggested upon discharge at low potentials [32,33]. The fact that two of the first discharge curves for the Li/CuO thin film cells considerably exceed the nominal capacity of the electrodes can also be explained by assuming the electrolyte to be reduced at potentials below 0.5 V. Both electrodes possess a high electrolyte/active material ratio, which may favour the electrolyte reduction.

In order to shed some light on these electrochemical processes, additional data were obtained by combining the step potential electrochemical spectroscopy (SPES) technique with ex situ XRD, XPS, and AFM measurements. Taking into account that the amount of lithium removed in the first charge was similar to that inserted in the second discharge (Fig. 4), the comments on the SPES curves will be restricted to these processes. Fig. 5a shows the SPES curves for the Li/sample A cell. The main feature of the first anodic curve is the presence of two doublets centred at 1.2 and 2.6 V. The second cathodic curve exhibits a weak peak at 2.35 V followed by a stronger band at 1.3 V and two broad overlapping peaks at 0.85 and 0.55 V. A fifth unresolved peak appears to exist below 0.0 V. Further cycling hardly alters the curve profiles, so the redox processes involving in the anodic and cathodic scans can be assumed to be reversible.

In order to more accurately assign the above-described peaks to the corresponding electrochemical reactions, two additional measurements were performed. Thus, the role of the electrolyte was elucidated, in a potentiometric study of the cell, using the substrate without active material as electrode. The SPES curves thus obtained are shown in Fig. 5b. Only two weak peaks at 0.5−0.6 and 0.9 V in the cathodic and anodic scan, respectively, were seemly obtained upon repeated cycling the origin of which might be an electrolyte decomposition redox process. As the formation/dissolution process of an SEI film around the metallic grains has been suggested to occur on the basis of the nanometric morphology of the active material, it is reasonable to think that degradation of the electrolyte might not be as intense if highly crystalline CuO is used as active material. The corresponding SPES curves of the cell are shown in Fig. 5c. The second cathodic curve resembles that exhibited by the film (see Fig. 5a); on further cycling,

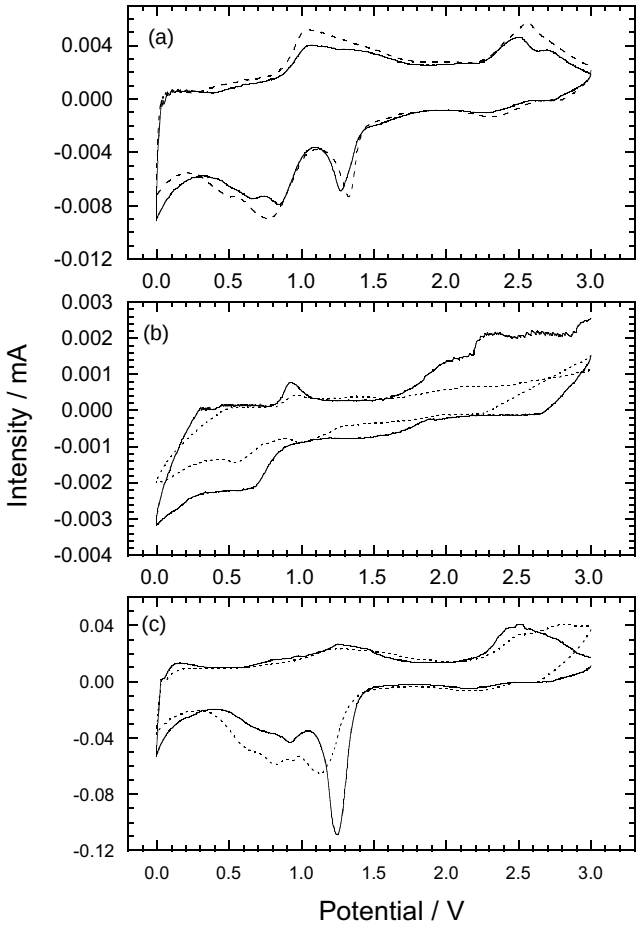


Fig. 5. SPES curves obtained for: (a) Li/sample A; (b) Li/substrate; (c) Li/bulk CuO cells. Measurements correspond to the second (—) and fifth (· · ·) discharge and charge of the cells.

however, the curve profile undergoes some shifts (specifically the peak at 1.25 V decreases in intensity and shifts to lower potentials). This suggests a decreased reversibility in the electrochemical reactions relative to the film. Furthermore, the peaks in the anodic curves are broader and weaker than those for the discharge process.

Fig. 6 shows the ex situ XRD patterns recorded at different discharge and charge potentials for the Li/sample B cell. At 1.5 V, the XRD pattern is similar to that for the pristine sample. This means that CuO apparently remains inactive and the signal above this potential can be associated to the formation of the SEI resulting from the reduction of the electrolyte solvent. On further discharge at 1.0 V, the diffraction lines for CuO disappear and a broad band at 36.6° $2\theta$ appears the origin of which may be $Cu_2O$ formation. This peak disappears at the end of the reduction process. Unfortunately, the expected copper diffraction lines at 0.0 V were indistinguishable owing to the similar spacing of the main peaks and those of the substrate among other reasons. All XRD patterns recorded at different cut-off potentials during the charge process had a very low signal-to-noise ratio, thus precluding the identification of any phases. Only for the fully

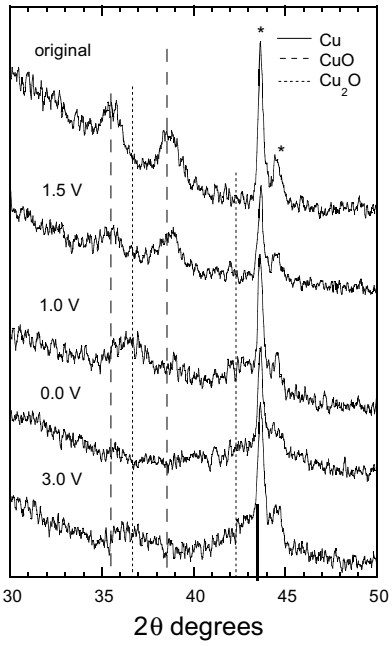


Fig. 6. Ex situ XRD patterns for sample B recorded at different discharge cut-off potentials. The pattern for the film charged up to 3.0 V is also shown.

charged electrode at 3.0 V was a subtle signal observed below 36° $2\theta$ that could be assigned to a phase related to copper oxides. Ex situ XPS spectra of the electrode after the first charge (cut-off voltage 3.0 V; Fig. 3d) revealed the presence of $Cu^{2+}$ at the electrode surface. The values of the binding energies for Cu $2p_{3/2}$ and $2p_{1/2}$ together with the shake-up satellite structure, rule out the presence of $Cu_2O$—at least in appreciable amounts. These data provide strong evidence of the reversibility of the reaction:

$$CuO + 2Li \Leftrightarrow Cu + Li_2O, \quad (2)$$

if CuO is prepared as thin electrode.

The involvement of the electrolyte in the electrochemical process was also apparent from the AFM images taken at different cut-off potentials. Fig. 7a shows the surface image of the electrode discharged at 1.5 V. As can be seen, the pristine roughness surface is hidden by a smooth film probably formed through electrolyte degradation at the beginning of the first discharge process, consistent with the 1.7 V peak in the corresponding SPES curve. This film persists throughout the discharge process but disappears on charging the cell. This means that, in the charge process, the SEI film is dissolved below 1.7 V (Fig. 7b) and round-shaped grains agglomerate again.

Fig. 8 shows the electrochemical response of samples A and F on cycling. As stated earlier, the specific capacity delivered by the sample A was initially higher than the theoretical value of reaction (2), 674 Ah $kg^{-1}$. Also, this sample exhibited the best electrochemical properties on cycling, with a high, constant specific capacity value of 625 Ah $kg^{-1}$ over 100 cycles. Such a high value may be related to the presence of $Cu^{2+}$ in the full charge state, in

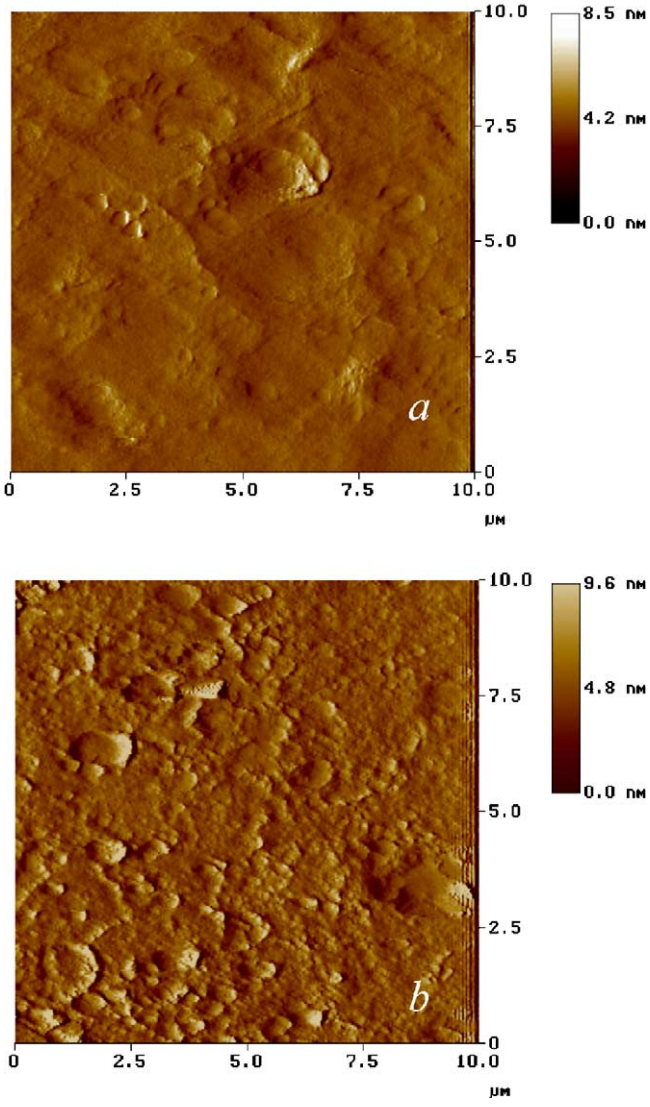


Fig. 7. AFM images for sample B: (a) discharged up to 1.5 V; (b) charged up to 1.7 V.

agreement with the data reported in [21]. Additional evidence to support this assumption was obtained from the above commented XPS spectra of Fig. 3d, consistent with

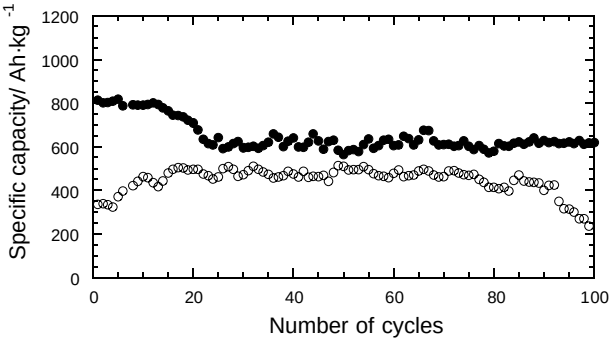


Fig. 8. Cycling properties of Li/CuO thin film cells: (●) sample A; (○) sample F.

the presence of $Cu^{2+}$ and not with $Cu^{+}$. The cycling properties of these CuO thin film electrodes differ from those reported for bulk CuO [10]. First, the discharge capacity delivered by the latter system was only ca. 400 Ah $kg^{-1}$, which is somewhat greater than the theoretical capacity of $Cu_2O$ (375 Ah $kg^{-1}$). This means that the oxidation reaction $Cu^{+} \rightarrow Cu^{2+}$ is kinetically hindered and that the electrochemical process on cycling is essentially controlled by the $Cu_2O$/Cu couple. Moreover, the cycling properties of the cell improved with increase in CuO particle size. Our electrodes can deliver more than 600 Ah $kg^{-1}$, close to the theoretical value for CuO—particularly the electrode featuring smallest particle size. We believe this unusual behaviour can be ascribed to two features. First, the nanometric size of the particles may enhance electrochemical activity in the film. Second, the good contact of the film with the substrate may facilitate the electron transfer at the active material–substrate interface. Indeed, this in an advantage of these electrodes, which can deliver a high capacity on prolonged cycling without the need to use an electron conductor additive such as carbon black. With a thick electrode of a large particle size (sample F), the specific capacity delivered by the cell in the first cycles is close to 400 Ah $kg^{-1}$, which is close to the theoretical value for $Cu_2O \Leftrightarrow Cu$ reaction, but then increases to ca. 500 Ah $kg^{-1}$, so not every Cu atom is oxidized to $Cu^{2+}$. In addition to the greater size of the particles, probably the nanoparticles located at a long distance from the substrate may find some difficulty in accomplishing a complete electron transfer because of the limited electronic conductivity of copper oxides. In any case, the specific capacity of the thickest film clearly exceeded that delivered by submicronic bulk CuO (400 Ah $kg^{-1}$) [10].

## 4. Conclusions

Spray pyrolysis of aqueous copper acetate solutions is a simple, effective method for preparing CuO thin films at moderate temperatures. At 200 °C, the organic salt is virtually decomposed and the substrate is thoroughly coated with a highly uniform, homogeneous film consisting of nanometric particles pseudo-spherical in shape. Under these conditions, CuO was the sole crystalline phase detected in the film; however, the XPS spectra revealed a more complex surface structure due to the presence of a small amount of undecomposed copper acetate—which can be easily removed by $Ar^{+}$-ion sputtering—and of $Cu_2O$ resulting from the reduction of $Cu^{2+}$ by X-rays. These films can react reversibly with lithium in a Li/$LiPF_6$, EC–DEC/film cell configuration over the potential range 0.0−3.0 V, the electrochemical performance of the cell improving with decreasing particle size and film thickness. Moreover, the cycling properties of these nanostructured CuO thin film electrodes differ from those reported for micrometric bulk CuO. Whereas this material has the ability to deliver a capacity of 400 Ah $kg^{-1}$, basically corresponding to the $Cu_2O \Leftrightarrow Cu$ redox reaction, the capacity of these films can be as high as 625 Ah $kg^{-1}$, which is only possible from a $CuO \Leftrightarrow Cu$ redox reaction. This value is maintained on prolonged cycling. The good capacity retention of the cells make these films attractive candidates as anodes for thin film Li-ion batteries.

## Acknowledgements

This work was funded by Junta de Andalucía (Group FQM-175) and Spain's Ministry of Science and Technology (Project MAT2002-04477-C02-02).

## References

[1] Y. Idota, M. Mishima, M. Miyaki, T. Kubota, T. Misayaka, European Patent Application 651450 A1 950503.
[2] Y. Idota, T. Kubota, A. Matsufuji, Y. Maekawa, T. Misayaka, Science 276 (1997) 1395.
[3] I.A. Courtney, W.R. McKinnon, J.R. Dahn, J. Electrochem. Soc. 146 (1999) 59.
[4] J. Morales, L. Sánchez, J. Electrochem. Soc. 146 (1999) 1640.
[5] H. Li, X. Huang, L. Chen, Z. Wu, Y. Liang, Electrochem. Solid-State Lett. 2 (1999) 547.
[6] J. Yang, M. Wachtler, M. Winter, J.O. Besenhard, Electrochem. Solid-State Lett. 2 (1999) 161.
[7] O. Mao, J.R. Dahn, J. Electrochem. Soc. 146 (1999) 423.
[8] K.D. Kepler, T. Vaughey, M.M. Thackeray, Electrochem. Solid State Lett. 2 (1999) 307.
[9] P. Poizot, S. Laruelle, S. Grugeon, L. Dupont, J.M. Tarascon, Nature 407 (2000) 496.
[10] S. Grugeon, S. Laruelle, S.R. Herrera-Urbina, L. Dupont, P. Poizot, J.M. Tarascon, J. Electrochem. Soc. 148 (2001) A285.
[11] D. Larcher, G. Sudant, J.B. Leriche, Y. Chabre, J.M. Tarascon, J. Electrochem. Soc. 149 (2002) A234.
[12] J. Schoonman, Solid State Ionics 5 (2000) 135.
[13] G.X. Wang, Y. Chen, K. Konstantinov, M. Lindsay, H.K. Liu, S.X. Dou, J. Power Sources 109 (2002) 142.
[14] Z. Yuan, F. Huang, C. Feng, J. Sun, Y. Zhou, Mater. Chem. Phys. 79 (2003) 1.
[15] F. Badway, I. Plitz, S. Grugeon, S. Laruelle, M. Dollé, A.S. Gozdz, J.M. Tarascon, Electrochem. Solid-State Lett. 4 (2002) A115.
[16] D. Larcher, M. Masquelier, C.D. Bonnin, Y. Chabre, V. Masson, J.B. Leriche, J.M. Tarascon, J. Electrochem. Soc. 150 (2003) A133.
[17] M.N. Obrovac, R.A. Dunlap, R.J. Sanderson, J.R. Dahn, J. Electrochem. Soc. 148 (2001) A576.
[18] S. Morzilli, B. Scrosati, F. Sgarlata, Electrochim. Acta 30 (1985) 1271.
[19] P. Novák, Electrochim. Acta 30 (1985) 1687.
[20] P. Novák, Electrochim. Acta 31 (1986) 1167.
[21] A. Débart, L. Dupont, P. Poizot, J.B. Leriche, J.M. Tarascon, J. Electrochem. Soc. 148 (2001) A1266.
[22] M. Cruz, L. Hernán, J. Morales, L. Sánchez, J. Power Sources 108 (2002) 35.
[23] J. Morales, L. Sánchez, F. Martín, J.R. Ramos-Barrado, M. Sánchez, J. Electrochem. Soc. 151 (2004) A151.
[24] R. Ayouchi, F. Martín, J.R. Ramos-Barrado, M. Martos, J. Morales, L. Sánchez, J. Power Sources 106 (2000) 106.
[25] ICDD card no. 45-937.
[26] R. Ayouchi, F. Martín, D. Leinen, J.R. Ramos-Barrado, J. Cryst. Growth 246 (2002) 191.

[27] B. Timmermans, F. Reniers, A. Hubin, C. Buess-Herman, Appl. Surf. Sci. 144–145 (1999) 54.
[28] J.F. Moulder, W.F. Stickle, P.E. Sool, K.D. Bomber, Handbook of X-ray Photoelectron Spectroscopy, Perkin-Elmer, Eden Prairie, 1992.
[29] E. Cano, C.L. Torres, J.M. Bastisdas, Mater. Corros. 52 (2001) 667.
[30] E. György, A. Pérez del Pino, P. Serra, J.L. Morenza, Surf. Coat. Technol. 173 (2003) 265.
[31] B. Laik, P. Poizot, J.M. Tarascon, J. Electrochem. Soc. 149 (2002) 251.
[32] E. Strauss, D. Golodnitsky, E. Peled, Electrochim. Acta 45 (2000) 1519.
[33] D. Aurbach, A. Zaban, Y. Ein-Ein, I. Weissman, O. Chusid, B. Markovsky, M. Levi, E. Levi, A. Schechter, E. Granot, J. Power Sources 68 (1997) 91.